Numerical Optimization of Plasmid DNA Delivery Combined with Hyaluronidase Injection for Electroporation Protocol

Daniele Peri[(1)], Manon Deville[(2)], Clair Poignard[(2)], Emanuela Signori[(3)], Roberto Natalini[(1)]

[(1)]*:CNR-IAC – National Research Council, Istituto per le Applicazioni del Calcolo "Mauro Picone" Via dei Taurini 19, 00185 Rome, Italy*

[(2)]*:Team MONC, INRIA Bordeaux-Sud-Ouest, Institut de Mathématiques de Bordeaux, CNRS UMR 5251 & Université de Bordeaux, 351 cours de la Libération, 33405 Talence Cedex, France*

[(3)]*:CNR-IFT – National Research Council - Istituto di Farmacologia Traslazionale, Via Fosso del Cavaliere 100, 00133 Rome, Italy*

d.peri@iac.cnr.it and emanuela.signori@ift.cnr.it

Abstract

Background and Objective: The paper focuses on the numerical strategies to optimize a plasmid DNA delivery protocol, which combines hyaluronidase and electroporation.

Methods: A well-defined continuum mechanics model of muscle porosity and advanced numerical optimization strategies have been used, to propose a substantial improvement of a pre-existing experimental protocol of DNA transfer in mice. Our work suggests that a computational model might help in the definition of innovative therapeutic procedures, thanks to the fine tuning of all the involved experimental steps. This approach is particularly interesting in optimizing complex and costly protocols, to make in vivo DNA therapeutic protocols more effective.

Results: Our preliminary work suggests that computational model might help in the definition of innovative therapeutic protocol, thanks to the fine tuning of all the involved operations.

Conclusions: This approach is particularly interesting in optimizing complex and costly protocols for which the number of degrees of freedom prevents a experimental test of the possible configuration.

1. Introduction

DNA delivery consists in injecting engineered DNA plasmid vectors carrying nucleotide sequences coding therapeutic molecules, so that transfected cells can work as factory to produce locally or systematically specific products to correct pathological defects Wolff et al. (1990). It has a deep potential in revolutionizing therapeutic treatments in the field of monogenic, polygenic, infectious and cancer diseases, as demonstrated in past and recent studies Hardee et al. (2017). However, the clinical use of DNA transfer protocols is still very

limited. Even though the efficacy has been proven in small animals studies, further improvements of DNA delivery and gene expression have to be performed before a standardisation of these treaments for humans Al-Dosari and Gao (2009).

1.1. DNA transport: a path full of pitfalls

DNA delivery is limited by the transport of the plasmid through the Extra-Cellular Matrix (ECM) and through the cell membranes to reach the cell nucleus for the gene expression Notarangelo et al. (2014). Indeed, ECM consists of a structural collagen network embedded in a gel of glycosaminoglycans (GAGs) and proteoglycans, which prevents the free diffusion of macromolecules such as plasmid vectors. Worstly, nuclease enzymes, which degrade the DNA, are present in the ECM Bureau et al. (2004). In addition, the cell membrane, which consists of a phospholipid bilayer with proteins, yields a barrier that have to be permeabilized to allow DNA penetration inside the cell.

A lot of bioengineering strategies are still under investigation for encompassing these two barriers. On one hand, the administration of hyaluronidase – an enzyme able to digest the ECM – before the DNA injection improves the plasmid distribution within the tissue Buhren et al. (2016); Girish and Kemparaju (2007). On the other hand, electroporation (EP), which consists in permeabilizing the cell membrane by mean of electrical short pulses, enables the penetration of non permeant molecules such as DNA Aihara and Miyazaki (1998); Rols et al. (1998); André and Mir (2004). The combination of hyaluronidase injected before the intramuscular DNA injection by electroporation has been shown to improve the DNA delivery and the gene expression as discussed in several papers. One can cite for instance McMahon et al. (2001); Schertzer et al. (2006); Chiarella et al. (2013b); Chiarella and Signori (2014); Akerstrom et al. (2015). Moreover, the role of hyaluronidase in improving DNA immunization protocol by EP has been largely discussed in Chiarella et al. (2013a); De Robertis et al. (2018). Interestingly, the experimental study of Mac Mahon *et al.* have demonstrated the differences in gene expressions due to time interval between intramuscular DNA injection and application of electric fields McMahon et al. (2001). Even though the link between DNA transfer and gene expression is still not well understood, these results suggest that it is possible to optimize the experimental protocols to maximize the DNA delivery for an higher gene expression also by mathematical studies Leguèbe et al. (2017).

1.2. Experimental protocol and degrees of freedom for optimizing DNA transfection

Our paper focuses on the specific experimental protocol on mice, which has been proposed by Chiarella and Signori Chiarella and Signori (2014). The experimental set-up consists in combining hyaluronidase injection, an enzyme which degrades the ECM improving the diffusion in the muscle, with electroporation right after the DNA injection to vectorize the DNA within the permeabilized cells.

More precisely, the intramuscular DNA transfection is performed in 3 steps as schematized by Figure 1. First, 10 units of bovine hyaluronidase in 25μl of buffer solution are injected by intramuscular injection during a few seconds T_{Hy}. After a waiting period of about 1h 30', 30μl of DNA (50μg) is injected at the same location as the hyluronidase during an injection

time T_{DNA} . Then electroporation is performed a few seconds ΔT_{EP} after the DNA injection. The gene expression is verified 3-5 days later.

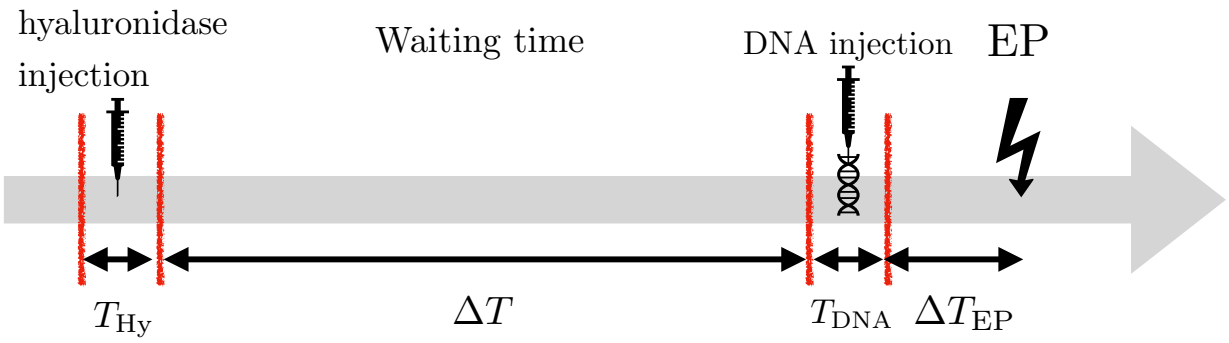

Figure 1: Time schedule of the experimental protocol.

Many parameters might be adjusted, such as the concentration of hyaluronidase and DNA, the choice of the muscle to be transfected, the electric pulse parameters and the injection speed André et al. (2006); Pucihar et al. (2011). However in order to minimize the modifications of the experimental protocol, and to propose realistic optimized protocols, we focus on the following 5 degrees of freedom. They consist in the times for both hyaluronidase and DNA injections T_{Hy} and T_{DNA} respectively, the waiting times ΔT and ΔT_{EP}, and the depth of the site of the intramuscular injection D_{inj} which is about 1 centimeter deep.

1.3. Goal of the computational study and paper organisation

The aim of this work is to investigate thanks to well-defined numerical algorithms, the influence of the 5 above degrees of freedom to optimize the distribution of DNA within the muscle, and to propose a realistic optimization of the experimental set-up protocol.

This numerical study is based upon the continuum mechanics model of enzyme-based tissue degradation combined with therapeutic molecule proposed by Deville *et al.* Deville et al. (2018). Interestingly, numerical optimization algorithms are shown to be an appropriate tool to optimize the experimental protocol set-up by maximizing the DNA distribution within the muscle. This has a deep potential since it could lead to the optimization of the DNA delivery.

The paper is organized as follows. Section 2 presents the mathematical and numerical methods proposed in the article to tackle the optimization problem. The mathematical model is presented in Subsection 2.1. The model has been proposed by Deville *et al.* in a dimensionless formulation Deville et al. (2018). The link between the dimensionless parameters and the physical parameters, as well as the values of the fixed parameters are also presented. The numerical methods regarding the computation of the the partial differential equations on the one hand and on the optimization strategy on the other hand are given in Section 2.2. Then the results are presented in Section 3. An optimized and realistic protocol is proposed to improve the DNA distribution with the muscle, before electroporation. According to the numerical results, it is possible to increase of 30% the DNA distribution,

which could improve a lot the DNA delivery, even though the link between the amount of vectorized DNA and gene expression is still unclear. The paper ends with some conclusions and future perspectives.

2. Material and Methods

A mathematical model, describing the different phases of the dosing regimen, represents a strong and powerful tool for the determination of the correct execution of the different actions to be taken during the administration protocol. In particular, starting form the analysis produced in Deville (2017), we have observed how some parameters are not optimally selected, although they appears to be able to change deeply the final effect of the whole procedure. Some experimental trials have been produced in order to drive the selection of the best values, but the number of attempts is clearly limited by the costs of the experimental activity, and the final result can be reasonably further improved. Under this perspective, the use of a mathematical model would be of great aid.

2.1. The poroelastic model of Deville et al.

In this section, we present the enzyme-based tissue degradation model recently proposed by Deville *et al.* in Deville et al. (2018). Modeling the behavior of porous media in which different continua interact at the microscopic level is not an easy task. In the current literature the mechanics of a porous medium is typically described by two different approaches: the averaging approach and the macroscopic approach Ambrosi et al. (2002), also known as mixture theory. The basic premise of the mixture theory is that the space occupied by a mixture is occupied co-jointly by the various constituents of the mixture, each considered as a continuum of its own. At any point of the space occupied by the mixture, there will be a particle belonging to each constituent Fusi et al. (2006); Chapelle and Moireau (2014). The model of Deville *et al.* combines the poroelastic theory of mixtures with the transport of enzymes and DNA plasmid densities in the extracellular space. The effect of the hyaluronidase on the tissue porosity and the mechanical response of the muscle are also accounted for.

2.1.1. Heuristics of the model

The rationale of the model is schematically described in Figure 2. The biological tissue is considered as a binary mixture of a solid and an interstitial fluid. The solid phase consists of cells and extracellular matrix (ECM) for which mass and momentum balance laws are written. The specificity of the model of Deville *et al.* lies in the fact that it accounts for the change of porosity due to the effect of hyaluronidase, which degrades the extracellular matrix.

The governing equations are set in the fixed reference domain –the tissue at the initial time– denoted by Ω_0. For the sake of simplicity, we assume that our system undergoes very small perturbations (see Deville et al. (2018) for more details).

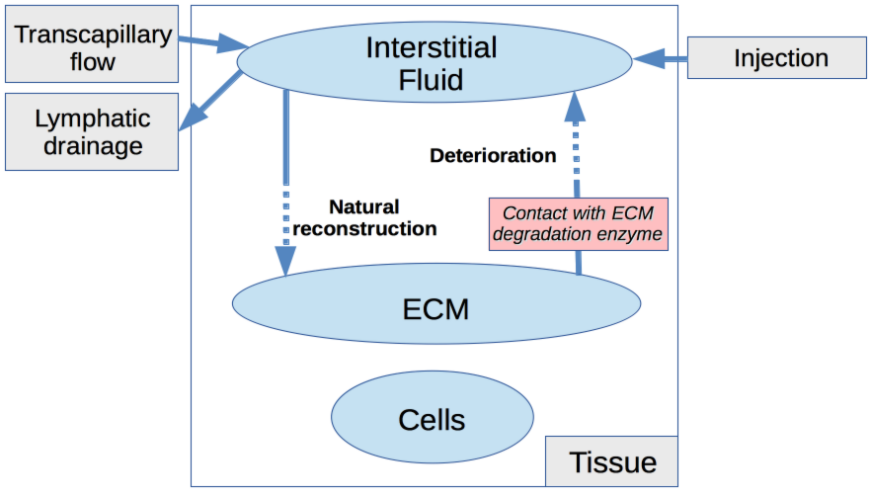

Figure 2: Schematic description of exchange pathways and production terms of the different phases. From Deville et al. (2018).

2.1.2. Mathematical statement of the model

The poroelastic model of Deville *et al.* describes the behavior of the volume fractions of ECM, cells and fluid –namely the blood in the tissue– denoted respectively by $g_{\mathcal{E}}$, $g_{\mathcal{C}}$ and f, as well as the evolution of the hyaluronidase concentration h and the DNA concentration denoted by c. The displacement vector, due to fluid injection is denoted by $\mathbf{u}$, and P is the inner pressure within the tissue. The dimensionless model reads as follows

$$
\begin{cases}
g_{\mathcal{E}} + g_{\mathcal{C}} + f = 1, & \text{(1a)}\\
\boldsymbol{\nabla} \cdot \left((g_{\mathcal{E}} + g_{\mathcal{C}}) \left(\overline{\lambda} (\nabla \cdot \mathbf{u}) I + \overline{\mu} (\nabla \mathbf{u} + \nabla \mathbf{u}^T) \right) \right) = \nabla P, & \text{(1b)}\\
(g_{\mathcal{E}} + g_{\mathcal{C}}) \overline{s_0} \dfrac{\partial P}{\partial t} - \nabla \cdot (\overline{\boldsymbol{\kappa}} \nabla P) = \alpha \, Q_{\text{inj}}^{\text{tot}} + \overline{\gamma} (\overline{P_v} - P) \\
\qquad\qquad + \left(\dfrac{\rho_s^{R,0}}{\rho_f^R} - 1 \right) g_{\mathcal{E}} (\overline{K} h + \overline{a_r} (f^{\text{phys}} - f)), & \text{(1c)}\\
\dfrac{\partial g_{\mathcal{C}}}{\partial t} + \left(\overline{s_0} \dfrac{\partial P}{\partial t} \right) g_{\mathcal{C}} = 0, & \text{(1d)}\\
\dfrac{\partial g_{\mathcal{E}}}{\partial t} + \left(\overline{K} h + \overline{a_r} (f^{\text{phys}} - f) + \overline{s_0} \dfrac{\partial P}{\partial t} \right) g_{\mathcal{E}} = 0, & \text{(1e)}\\
\dfrac{\partial h}{\partial t} = \nabla \cdot (f \overline{\mathbf{D}_{\text{enz}}^0} \nabla h + h J_{\text{enz}}) - \dfrac{\overline{k_{\text{enz}}^d}}{f} h + \dfrac{\alpha \mathcal{S}_{\text{enz}}}{c_0}, & \text{(1f)}\\
\dfrac{\partial c}{\partial t} = \nabla \cdot (f \overline{\mathbf{D}_{\text{dna}}^0} \nabla c + c J_{\text{dna}}) - \dfrac{\overline{k_{\text{dna}}^d}}{f} c + \dfrac{\alpha \mathcal{S}_{\text{dna}}}{c_0}, & \text{(1g)}
\end{cases}
$$

where the fluxes of hyaluronidase and DNA concentrations are defined by

$$J_{\text{enz}} = \frac{1}{f}\overline{\boldsymbol{\kappa}}\,\nabla P - \overline{\mathbf{D}^0_{\text{enz}}}\nabla f \quad \text{and} \quad J_{\text{dna}} = \frac{1}{f}\overline{\boldsymbol{\kappa}}\,\nabla P - \overline{\mathbf{D}^0_{\text{dna}}}\nabla f. \tag{2}$$

The saturation assumption (1a) ensures that the tissue is composed by nothing else but ECM, cells and fluid. Elasticity equations with a slightly compressible cells phase are then set in (1b)–(1c). The evolution of the porosity of two phases (cells and ECM) are then given by (1d)–(1e). Equation (1f) describes the distribution and the effect of the hyaluronidase on the ECM porosity, while equation (1g) describes the distribution of DNA. The above partial differential equations (PDEs) system is complemented with initial and boundary conditions. Denote by Γ the boundary of the domain Ω_0. We generically denote by $\mathbf{n}$ the normal to Ω outwardly directed from the inside to the outside of the domain. We suppose that Γ is split into 2 parts denoted respectively by Γ_u and Γ_t (see Fig. 3). The following boundary conditions are imposed

$$\mathbf{S}^E_s\,\mathbf{n} = 0 \text{ on } \Gamma_t, \text{ and } \mathbf{u} = 0 \text{ on } \Gamma_u \tag{3}$$

$$P = 0 \text{ on } \Gamma_t \text{ and } \nabla P \cdot \mathbf{n} = 0 \text{ on } \Gamma_u, \tag{4}$$

$$\begin{cases} h = 0 \text{ on } \Gamma_t, & \text{(5a)} \\ \left(f\mathbf{D}^0_{\text{enz}}\nabla h + hJ_{\text{enz}}\right)\cdot\mathbf{n} = 0 \text{ on } \Gamma_u. & \text{(5b)} \end{cases}$$

The same type of boundary conditions are applied to DNA plasmid concentration:

$$\begin{cases} c = 0 \text{ on } \Gamma_t, & \text{(6a)} \\ \left(f\mathbf{D}^0_{\text{dna}}\nabla c + cJ_{\text{dna}}\right)\cdot\mathbf{n} = 0 \text{ on } \Gamma_u. & \text{(6b)} \end{cases}$$

The initial conditions are given in Table 1.

2.1.3. Dimensionless parameters, and values of the physical parameters

We can observe from equation 6 how the PDEs system involves a large number of parameters. Being the model dimensionless, it is important to recall the link between the dimensionless (with an overline) and the physical (without overline) parameters as given in Deville et al. (2018). We denote by l_0 the characteristic length of the tissue. The dimensionless Piola-Kirchhoff and Cauchy stress tensors are defined as $\overline{\mathbf{S}^E_s} = \mathbf{S}^E_s/(\lambda + 2\mu)$ and $\overline{\boldsymbol{\sigma}^E_s} = \boldsymbol{\sigma}^E_s/(\lambda + 2\mu)$, respectively, and we define the dimensionless parameters

$$
\begin{aligned}
&\overline{\mu} = \frac{\mu}{\lambda+2\mu}, && \overline{\lambda} = \frac{\lambda}{\lambda+2\mu}, && \overline{s_0} = s_0(\lambda+2\mu), && \overline{\boldsymbol{\kappa}} = \frac{1}{\kappa}\boldsymbol{\kappa},\\
&\alpha = \frac{l_0^2}{\kappa(\lambda+2\mu)}, && \overline{K} = \alpha c_0 K, && \overline{a_r} = \alpha a_r, && \overline{\gamma} = \frac{l_0^2}{\kappa}\gamma,\\
&\overline{\mathbf{D}^0_{\text{enz}}} = \frac{1}{\kappa(\lambda+2\mu)}\mathbf{D}^0_{\text{enz}}, && \overline{k^d_{\text{enz}}} = \alpha k^d_{\text{enz}}, && \overline{P_v} = \frac{P_v}{\lambda+2\mu},\\
&\overline{\mathbf{D}^0_{\text{dna}}} = \frac{1}{\kappa(\lambda+2\mu)}\mathbf{D}^0_{\text{dna}}, && \overline{k^d_{\text{dna}}} = \alpha k^d_{\text{dna}}.
\end{aligned}
$$

We choose the $(\lambda+2\mu)$ parameter as a natural pressure scale; by this choice the dimensionless elastic parameters $\overline{\lambda}, \overline{\mu}$ are of order 1 Lang et al. (2016). Some of the physical parameters can be found in the literature, and others depend on the experimental protocol. The physical parameters that are considered fixed are given in Table 1, where, if nothing is reported, correspond to the values proposed Deville et al. (2018).

Table 1: Values of the physical parameters fixed for the numerical parametric studies, see also Deville et al. (2018).

Parameter	Symbol	Value	Unit	Reference
Characteristic length of the muscle	l_0	10^{-2}	m	
Reference mass concentration	c_0	1	kg/m^3	
Density of fluid phase	ρ_f^R	10^3	kg/m^3	Yao et al. (2012)
Density of solid phase	$\rho_s^{R,0}$	1.09×10^3	kg/m^3	Ward and Lieber (2005)
Specific storage coefficient	s_0	10^{-6}	1/Pa	
Hyaluronidase injected mass concentration	$c^{\text{enz}}_{\text{inj}}$	8×10^{-3}	kg/m^3	McMahon et al. (2001)
Mass concentration of injected DNA at $T_{\text{Hy}}+\Delta T$	$c^{\text{dna}}_{\text{inj}}$	1.67	kg/m^3	Chiarella and Signori (2014)
Permeability	$\boldsymbol{\kappa}$	10^{-11}	m^2/Pa/s	Swartz and Fleury (2007)
Lamé first parameter	λ	7.14×10^5	Pa	Zöllner et al. (2012)
Lamé second parameter	μ	1.79×10^5	Pa	Zöllner et al. (2012)
Diffusion coefficient of the enzyme	$\mathbf{D}^0_{\text{enz}}$	10^{-4}	m^2/s	
Diffusion coefficient of the therapeutic agent	$\mathbf{D}^0_{\text{dna}}$	10^{-9}	m^2/s	
Starling's coefficient	γ	5×10^{-5}	1/Pa/s	Soltani and Chen (2012)
Fluid/solute coefficient	γ_c	0.9	-	Baxter and Jain (1989)
Measure of treatment efficacy	K	10^{-14}	m^3/s/U	
Recovery coefficient	a_r	5×10^{-4}	1/s	
Hyaluronidase degradation rate	k^d_{enz}	1×10^{-4}	1/s	
DNA degradation rate	k^d_{dna}	2×10^{-4}	1/s	
Driving pressure	P_v	10^{-1}	Pa	
Initial values	**Symbol**	**Initial value**	**Unit**	
Volume fraction of fluid	$\varphi_f(0,\mathbf{x}) = \varphi_f^{\text{phys}}$	0.1	-	
Volume fraction of ECM	$\varphi_{\mathcal{E}}(0,\mathbf{x})$	0.4	-	
Volume fraction of cells	$\varphi_{\mathcal{C}}(0,\mathbf{x})$	0.5	-	
Network dilatation	$\nabla\cdot\mathbf{u}(0,\mathbf{x})$	0	-	
Enzyme concentration	$h(0,\mathbf{x})$	0	U/m^3	
Concentration of DNA	$c(0,\mathbf{x})$	0	μ g/ μ L	
Initial pressure	$p(0,\mathbf{x})$	0	Pa	

2.2. Numerical methods

2.2.1. Finite Element Method to solve the PDE system

The numerical simulation of the effects of the complete dosing regimen is obtained by discretizing a portion of the tissue where the injections will be performed and observing the diffusion of the plasmid and the DNA in this volume, resolving the previously described systems of equations.

Given the value of all the parameters by Table 1, the aforementioned PDE system (1) has been implemented with the finite element method (FEM). For the sake of simplicity, the domain representing the tissue is half of a sphere, and thanks to symmetries, only a 2D axisymmetric version of system (1) is solved. The mesh has been generated with three-dimensional finite element mesh generator Gmsh Geuzaine and Remacle (2009). The mesh is refined in the vicinity of the injection point, in order to describe precisely the displacement (see Fig. 3). The flat top Γ_u represents the derma and the epiderma on which a free boundary value condition with no flux is imposed. The boundary Γ_t is assumed to be far enough from the injection point, so that the pressure and the normal component of the Cauchy stress tensor are set to zero. The details of the numerical schemes to solve the nonlinear model are provided in Section 4 of Deville et al. (2018). In Deville (2017) a sensitivity analysis of the grid density has been performed, in order to check the minimum grid density assuring the convergence (and stability) of the numerical solution. The following computations have been performed always using this grid density (around 8000 cells). The open-source library `FreeFEM++` Hecht (2012) as been used for the calculations. The code `FreeFEM++` has been run on a 2 x Xeon 18-Core 6140 2.3Ghz with 96GB RAM.

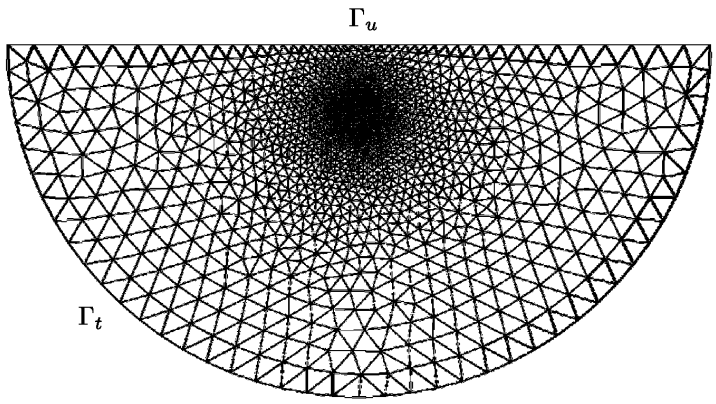

Figure 3: Computational grid for the poroelastic problem. The density of the mesh is increased in the vicinity of the injection point. The axisymmetric configuration of the half sphere is chosen to minimize the computational. The flat top Γ_u represents the derma and the epiderma on which a free boundary value condition with no flux is imposed.

2.2.2. Optimization method

The adopted optimization strategy is based on the general framework of the "Multi-point Approximation Method" Toropov (1995), or generally speaking the "Metamodel-Based Simulation Optimization" (see Barthelemy and Haftka (1993); Barton and Meckesheimer (2006)). This approach can be synthetically described as follows. The first step consists in the generation of a suitable number of *training points*, preferably regularly spaced, spanning the design variable space. The number of the training points is unknown *a priori*, depending typically on the rate of variation of the objective function and on the number of design variables. It can be fixed also considering the allowed computational effort for the optimization activities. The objective function is now computed at the training points, obtaining the so called *training set*. The training set is used in order to derive an interpolation/approximation of the objective function over the full design space, generally called *metamodel* (a model of the model). The metamodel is substantially an algebraic model, able to mimic the numerical response of the computationally expensive mathematical model. The training phase of the metamodel depends on the characteristics of the metamodel itself: during the training phase, the parameters of the metamodel are optimized in order to minimize the prevision error. Some metamodels are trained easily, *i.e.* by solving a linear system whose dimension is equal to the number of training points, other metamodels require the solution of an optimization algorithm (like neural networks). A small part of the training set can be put momentarily aside, forming the *verification set*, and then it can be used at the end of the training phase in order to verify the accuracy of the metamodel on positions not previously used during the training. Several techniques can be now adopted in order to select new training points with the aim of increasing the accuracy of the prediction, if required: examples are reported in Peri (2009); Shu et al. (2017). Once the quality of the metamodel is satisfactory, it can be applied to the optimization algorithm, in order to identify the optimal parameters of the mathematical model. Since the evaluation of the metamodel is computationally inexpensive if compared with the mathematical model, the overall computational cost of the optimization procedure is equal to the time of the training phase. In this paper, we selected the *Orthogonal Arrays* (OA) for the generation of the training set Hedayat et al. (1999). OA is a mathematically consistent methodology for the reduction of the number of the training points required by a generic metamodel (interpolation/approximation algebraic model). It is designed for preserving the orthogonality of the samples, starting from the classical L^k factorial design, where L is the number of subdivisions (levels) for each design variable and k is the number of the involved design variables. Since metamodels are generally very sensible to the uneven spacing of the training points, a random selection is inappropriate. There are plenty of other methodologies, equally effective, but in our experience, OA is a good choice in combination with the selected optimization strategy.

3. Results

3.1. Influence of the noise on the optimization - optimization criterion selection

The determination of the optimal values of the four parameters requires, in general, the application of an optimization algorithm: once a mathematical programming problem is

formulated, a large number of trial vectors of the design parameters need to be automatically generated and evaluated, as soon as the convergence to the optimal values of the parameters is obtained. We also need a quantity to be minimized/maximized in order to drive the selection of the best parameters, and the area reached by the DNA-plasmid is suitable to this goal. We thus define the effective area as the area where the concentration of the DNA-plasmid is higher than 5% of the injected concentration. The optimized configuration is defined as that configuration which maximizes the effective area. Due to the ECM nucleases, the injected plasmid is degraded and the effective area admits a maximum value, which can be determined numerically. In Figure 4 the typical profile of plasmid effective area is given.

Unfortunately, the numerical noise connected with the numerical solution of the problem and the large computational time required to finalize a single simulation represent two great obstacles in the application of this approach. In fact, a noisy behavior of the function to be minimized/maximized is typically creating a number of false minima/maxima, and the optimization algorithm is sometime trapped into those regions. Regarding the CPU time for the solution of a single configuration, depending on the values of the parameters, it could be greater than five hours, and around ten thousand of simulation are needed for reaching the convergence to the optimal solution in our case.

To give an example of the effects of the numerical noise, Figure 5 is reporting the effects of a very small variation of a single parameter while all the other parameters are kept fixed. The effect of the variation of a single parameter on the total effective area is reported in the corresponding sub-figure. The central value is representing one of the best configuration identified during the following exploration. We can observe how, in the investigated region, the time between the two injections is not changing at all the value of the effective area, while for the other parameters a nearly random effect is observed: it is evident that a sort of uncertainty is connected with the estimate of the effective area, and the simple punctual value provided by the simulation cannot be representative of the real effects of the selected parameters.

For this reason, we thus need to define a different value of the effective area, able to account for the not negligible local sensitivity to the parameters of the output of the simulations. We decided here to apply a worst case approach, and the average value of a group of local samples, reduced by the associated variance, is defined as our objective function. Statistically, the use of this quantity guarantees that the effective area in the neighborhood of the selected configuration of the dosing parameters is greater than the indicated value with a probability of 84.15%. From now on we will refer to the effective area as its average value (computed on a sampling set of 9 configurations) minus the variance.

In Figure 6 we have reported the full evolution curve of the effective area for the nine configurations adopted during the sensitivity analysis of a single simulated point. On left, the differences in absolute terms are reported, on the right the percentage differences are shown. Percentage differences are computed with respect to the value of the central point of the distribution. We can observe how a difference of about eight percentage points is recorded among the different curves. This represents a sign of great sensitivity of the simulation model to the parameter variation. The fluctuations are slightly amplified by the lower value

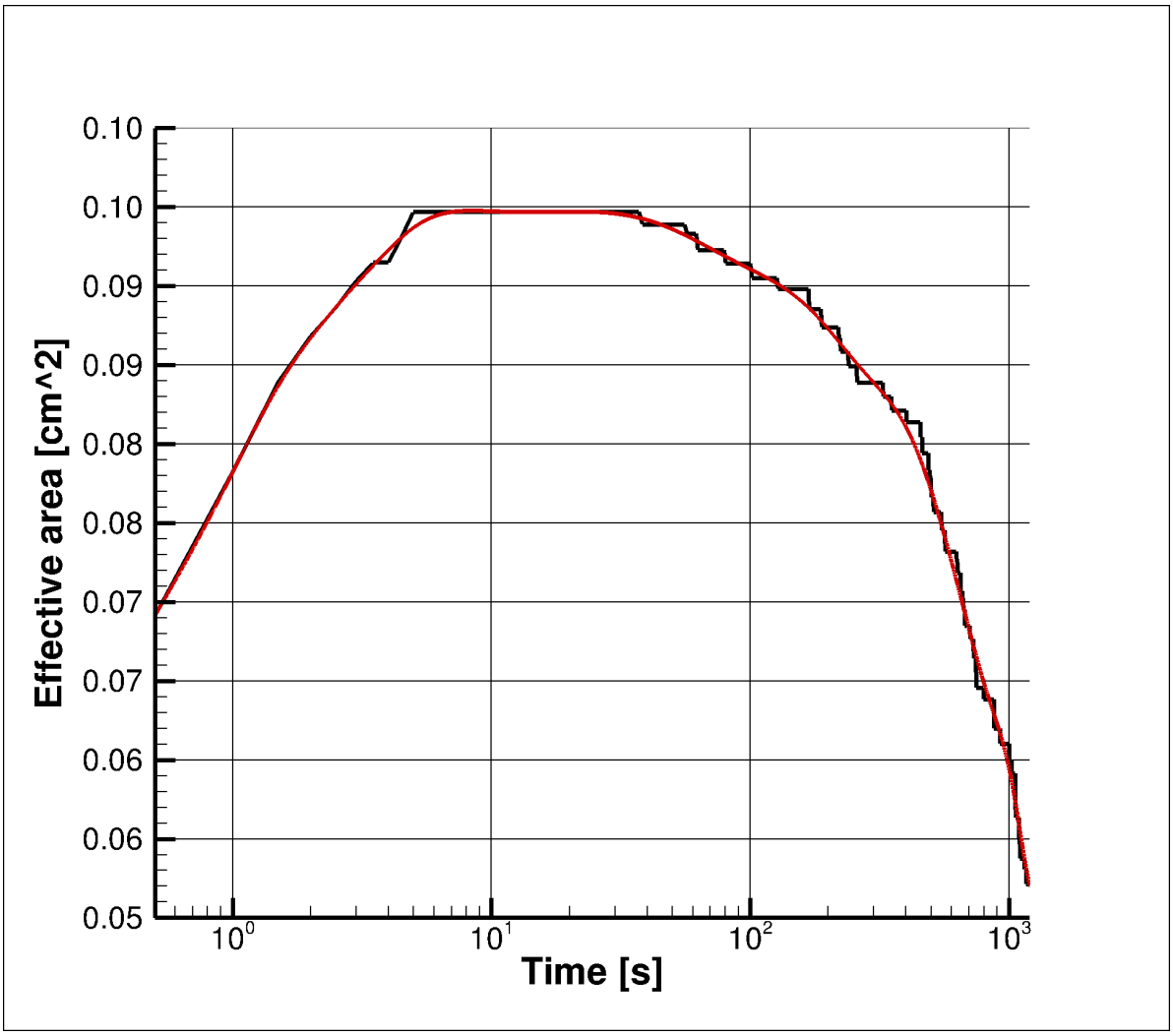

Figure 4: Typical profile of the evolution of the DNA area from the starting time to the end of the plasmid injection.

of the effective area at the end of the curve. This behavior represents a strong element for the consideration of an averaged value instead of a punctual value of the effective area.

3.2. Optimization method

The generation of the training set is obtained by the *Orthogonal Arrays* method presented in Hedayat et al. (1999). 16 levels for the regular subdivision of each direction of the design space have been selected. The OA criterion to reduce the number of sampling points from 65536 points to 512 sampling. Since we need to perform a sensitivity analysis for each sample point, the total number of configurations to be analyzed is 4608.

As a surrogate model, a multi-dimensional spline approximator Peri (2018) has been adopted, tuned using the results provided by the previously produced training set. The

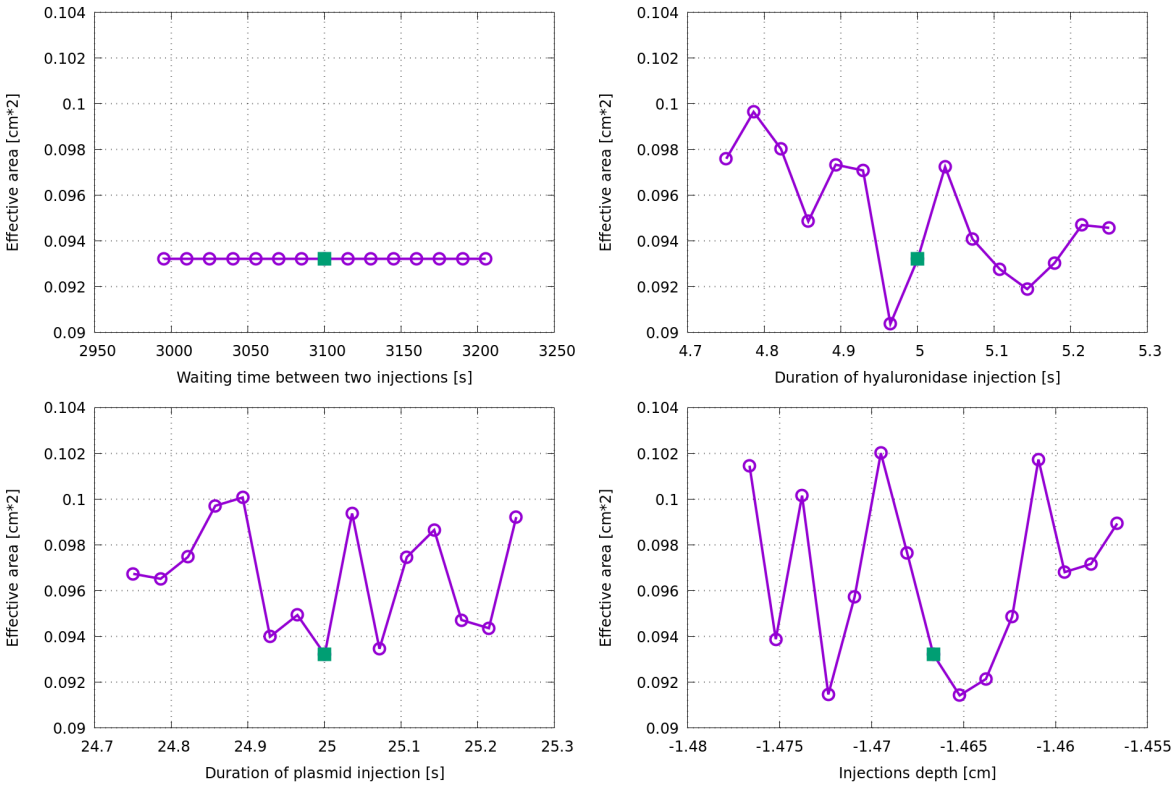

Figure 5: Sensitivity analysis of the area reached by the therapeutic agent as a function of the injection deepness only. On the left, comparison between the point values and the interpolated ones, on the right the interpolated values only (scales are different).

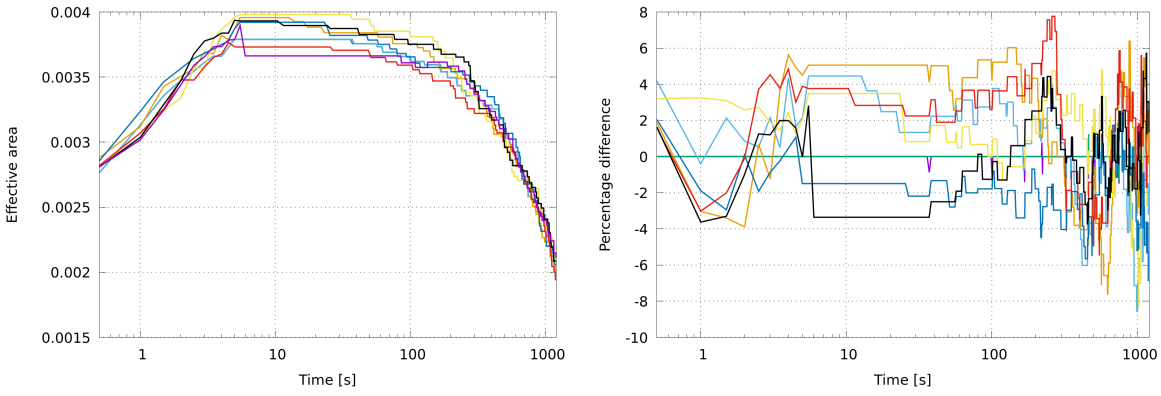

Figure 6: Absolute (left) and percentage (right) differences observed on the nine configurations adopted in the sensitivity analysis. Percentage differences are computed with respect to the central point of the distribution.

range of variation of each parameters has been prefixed as follows. ΔT is varied between 300 and 10800 seconds; T_{Hy} and T_{DNA} are varied between 5 and 30 seconds, and D_{inj} is varied between 1 and 2 centimeters. These values have been selected according to preliminary numerical experiences obtained by Deville Deville (2017).

In order to increase the credibility of the meta-model, some further training points have been added sequentially in those areas where the objective function appears to be favorable. The full number of training points, at the end of the refinement phase, has become 686 (6174 configurations). A solution of mathematical model is produced for the new training points, and the difference between the value of the objective function estimated by the meta-model and the real value provided by the mathematical model at the new point is assumed as the precision index of the meta-model. The history of the refinement phase is reported in Figure 7. Range of variations of the parameters are also adjusted.

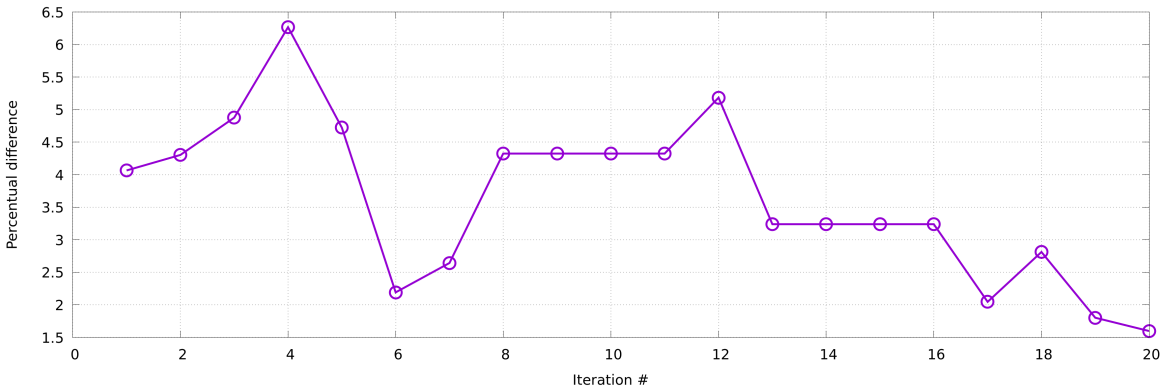

Figure 7: Precision index of the meta-model during the refinement phase.

The determination of the best configuration is obtained by regularly sampling the design space and then recursively refining the investigation as soon as the dimension of the investigated area is lower than a prescribed limit. Since this operation is completed by using the metamodel, we can adopt very strict parameters: we have here 51 subdivisions along each coordinate direction and the final spatial precision of the search is fixed at 10^{-8}.

3.3. Numerically optimal protocols

Figure 4 shows that the best value of ΔT_{EP} is about 30 seconds since the maximal effective area reaches a plateau after a few tens of seconds which lasts about 30 seconds. This is in line with the experimental constraints for the preparation of the EP set-up. If ΔT_{EP} is longer than 30-40 seconds, the protocol suffers for a reduction of efficacy.

Figure 8 and Figure 9 represents the parameters region of T_{Hy} , ΔT and T_{DNA} , for different depth of the injection point D_{inj} , for which the objective function is above 99% of the maximum observed value respectively 1min and 16 min after the end of the DNA injection.

If we are able to complete the preparation of the EP phase in 1 minute, the duration of the plasmid injection should be very small. From Figure 8 we can observe how the

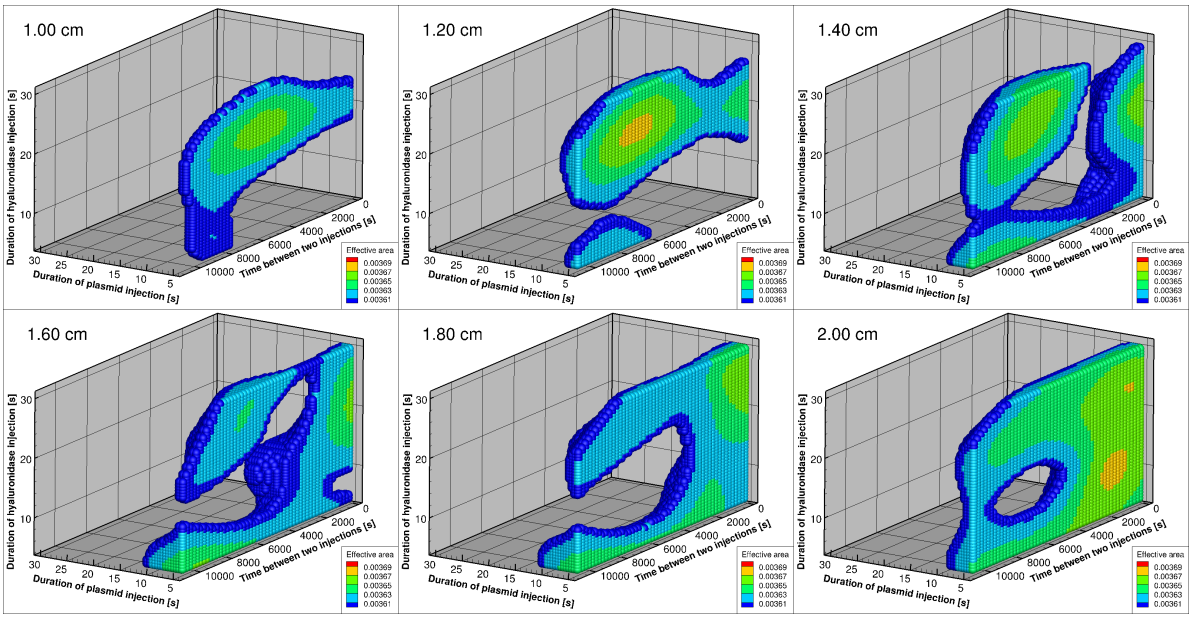

Figure 8: Range of parameters for which a loss of 1% with respect to the maximum realizable effective area is obtained. Time after the plasmid injection completion: 1 minute.

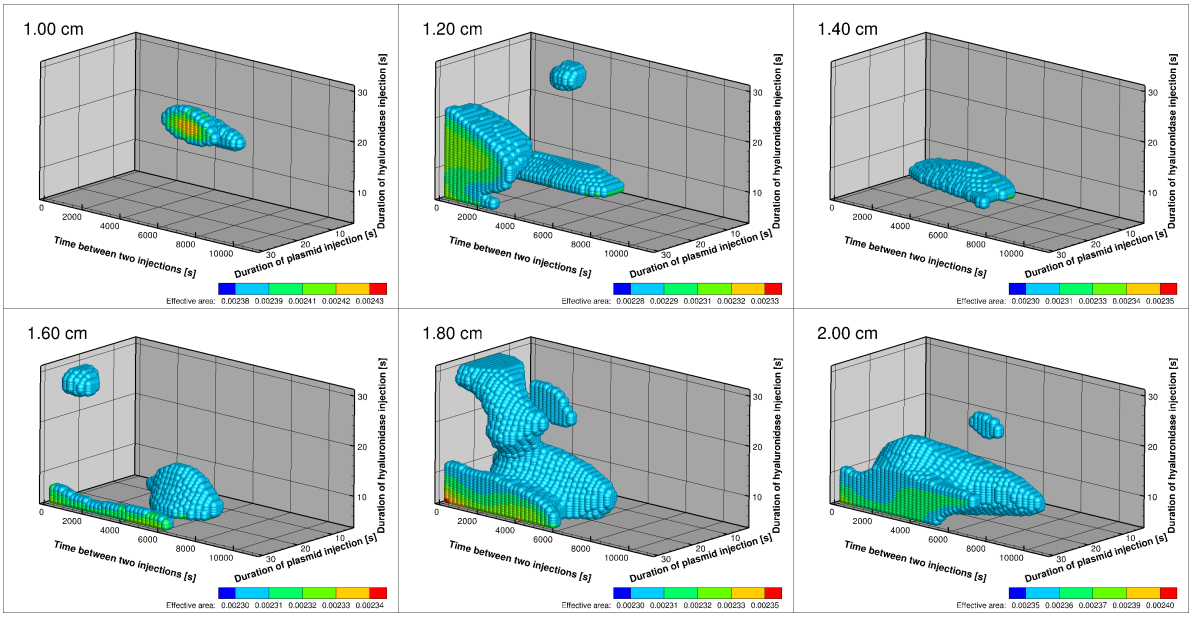

Figure 9: Range of parameters for which a loss of 1% with respect to the maximum realizable effective area is obtained. Time after the plasmid injection completion: 16 minutes.

preferable value of D_{inj} is not univocal, since similar values are obtained for 1.2 centimeters and 2 centimeters, but the values of ΔT are different, being shorter in the case of the deeper

injection. This may represent an advantage if several experiments are performed in series.

On the contrary, if we observe the results after 16 minutes, reported in Figure 9, the value of the objective function for the case of D_{inj} equal to 2 centimeters is larger than in the other cases. T_{DNA} can be longer, while ΔT is variable.

Figure 10 reports the optimal range of parameters when D_{inj} is fixed at 2 centimeters, when ΔT ranges from 1 min to 16 min. The scale of the objective function is changing from sub-picture to sub-picture.

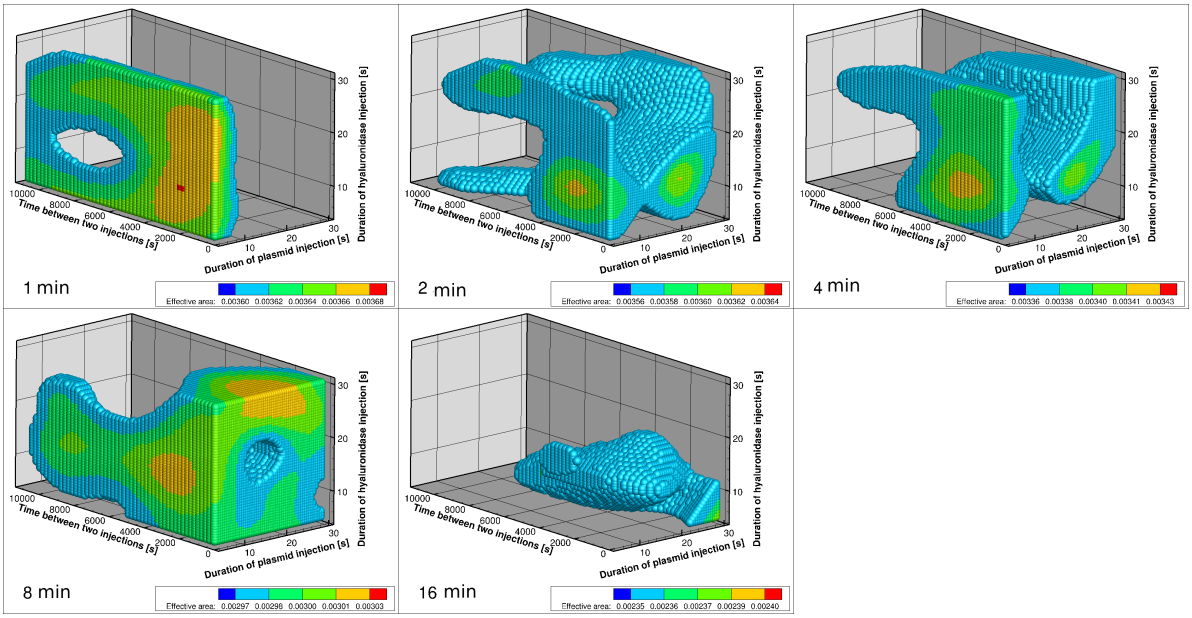

Figure 10: Range of parameters for which a loss of 1% with respect to the maximum realizable effective area is obtained. Depth of the injections: 2 centimeters.

After 8 minutes we have the larger tolerance in the best parameters: this area is largely reduced if the EP is performed after 16 minutes. At the same time, the objective function is reduced if the EP waiting time is increased. The numerical estimate of this loss is reported in Figure 11.

In order to quantify the improvements potentially obtained by the optimization procedure, a reference configuration, commonly adopted for this kind of experiments, has been compared with the best configuration identified by the optimization procedure. Results are reported in Figure 12. An increase of about 30% is obtained if the EP is performed after no more then 8 minutes from the DNA injection: in fact, it is obviously convenient to perform the EP at the moment of the maximum expansion of the DNA into the tissues. If the waiting time is greater than 10 minutes, the two different strategies does not show significant differences, probably because the dynamics connected with the degradation of the DNA are substantially independent from the protocol details. The observation of these results suggest not to delay the EP procedure after 30 seconds: this request may require the application of a fully automated operations, in order to reduce the time spent in all the different preliminary

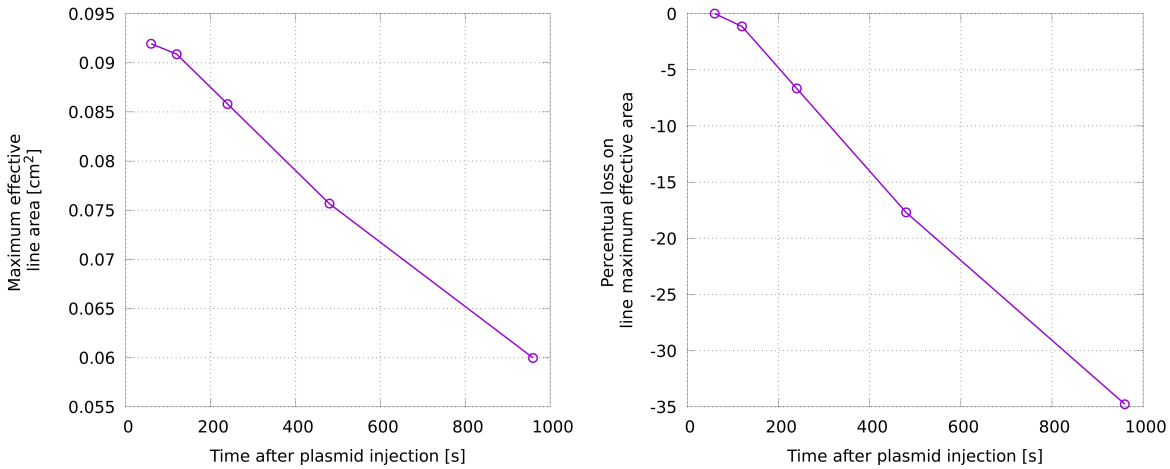

Figure 11: Loss in the effective area with an increasing ΔT. (Left): absolute values. (Right): percentage values.

sub-activities required by EP, such as correct immobilization of the subject undergoing to EP, application of conductive gel in the area to treat, correct placement of the electrodes, ...). This time reduction is of paramount importance since a longer waiting time is almost nullifying all the advantages obtained by the optimized protocol.

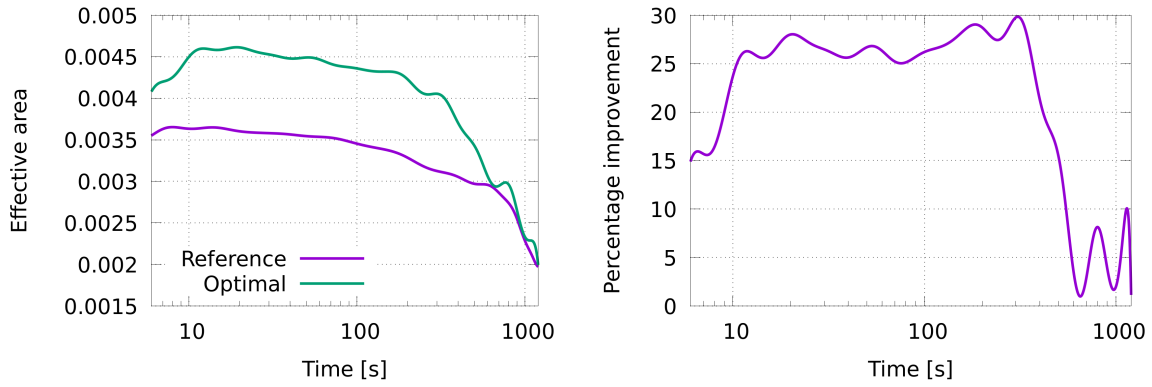

Figure 12: Comparison between a reference configuration and the overall optimal configuration identified by the numerical analysis.

4. Discussion

In the experimental protocol, a waiting time of 1h 30 between the two injections, of hyaluronidase and DNA, is adopted. Typically, T_{DNA} is about one or two hours later respect to the hyaluronidase administration. This has been motivated by the necessity to be sure

that the hyaluronidase has enough time to develop its effect, increasing the porosity of the ECM and then facilitating the access of the plasmid DNA at the border of the cells.

At the end of the solution of the optimization process, two categories of best solutions have been identified: the overall best configuration ever computed in terms of effective area and the best configuration in terms of objective function. The second solution is the preferable one, since it takes into account the variability of the effective area under small variations of the control parameters. The set of realized parameters differs largely between the two solutions: in particular, while in the first case ΔT is 3500 seconds, in the second case ΔT is nearly 300 seconds. This second option is absolutely preferable, since it reduces a lot the overall execution time of the experiment, but a deeper analysis is needed in order to understand why different timings led to similar results. In Figure 13, the elements for a reasonable explanation are reported. In the picture, we have plotted the porosity of the tissue at the time of the DNA-plasmid injection for the two different values of ΔT. In the same picture, the maximum expansion of the DNA-plasmid in the tissue is also reported, plotting the area in which the concentration of DNA-plasmid is more than 5%. We can observe how the effect of the hyaluronidase is clearly increasing with ΔT, since almost the whole computational volume has been interested by the action of the hyaluronidase when ΔT is 3500 seconds.

For the shorter value of ΔT, the same effect is obtained in the very central part of the computational volume, but the effect vanishes quickly. On the bottom part of Figure 13, the area in which we have a significant concentration of DNA-plasmid is reported: we can observe how this area is really small, so that the effect of the hyaluronidase in the case of the small ΔT is absolutely sufficient.

This result is connected with the large dimensions of the DNA-plasmid, and consequently its great difficulties in traveling into the ECM. Observing this result, we can argue that multiple injections of DNA-plasmid in a small area could probably increase (linearly with the number of injection sites) the overall effect of the protocol, since further modifications of the method of administration of the hyaluronidase appear not to be effective.

In Table 2, the exact values of the design parameters are reported for three different options for the protocol: the reference values (α), based on some indications about common practice adopted in pre-clinical protocols, the configuration providing the best overall value of the effective area (β) and the configuration maximizing the objective function (γ). Since the objective function is taking into account the stability of the solution in the neighborhood of the computational point, this last configuration is preferable. We can observe that, in the case α we have the maximum values for ΔT and D_{inj}, while T_{Hy} and T_{DNA} are the smaller ones. Both β and γ suggest a smaller value of ΔT, significantly shorter in the case γ. This is probably the more interesting result, since this allows for a huge compression of the overall duration of the experiment and gives also some indications about the behavior of the DNA-plasmid. T_{Hy} and T_{DNA} are larger for both β and γ with respect to α: due to the small injected quantities, probably the implementing rules suggested in β cannot be practically achieved. The smaller value of D_{inj} in β and γ, on the contrary, is compatible with the experimental setup.

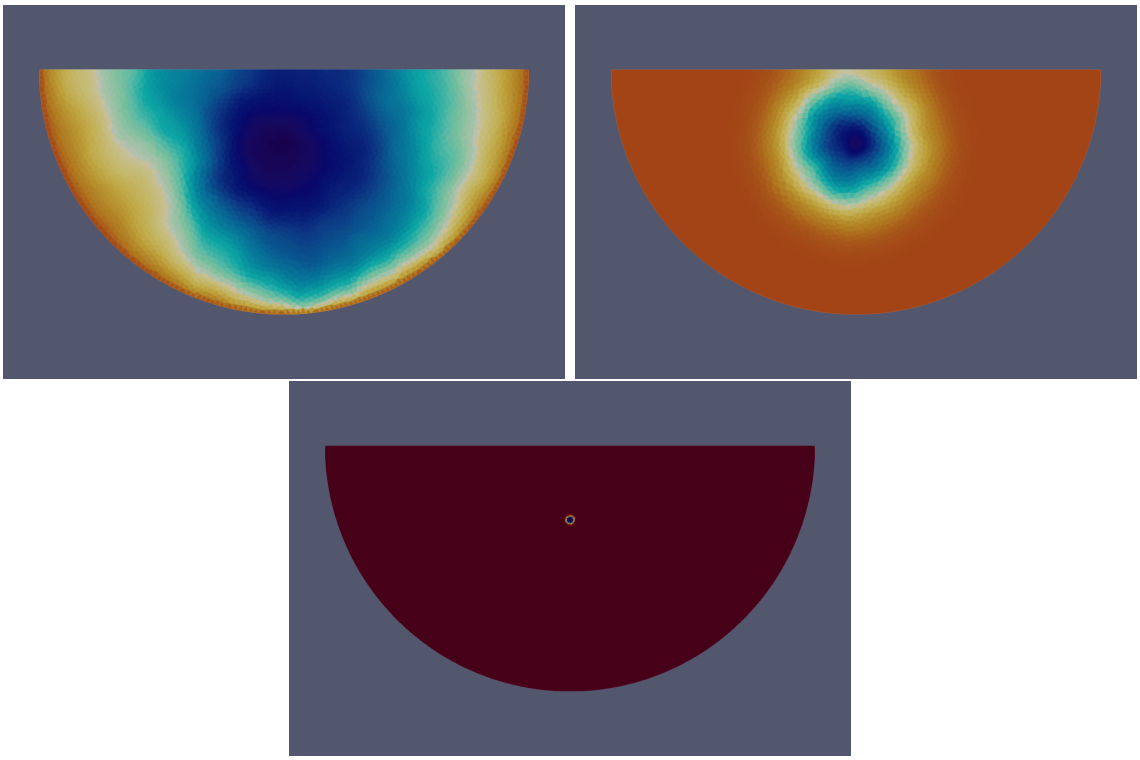

Figure 13: On top: Porosity variation in the computational domain at the corresponding ΔT. On left, ΔT is 3800 seconds, on right is about 290 seconds. On bottom, the maximum area where the concentration of the DNA-plasmid is larger than 5%.

Table 2: Values of the control parameters for three different configuration of the protocol: values in the standard experimental setup, best effective area (punctual value very sensitive), best objective function value (locally averaged value).

Parameter	Standard protocol	Best EA	Best OF
T_{Hy} [s]	10.00	28.33	21.47
ΔT [s]	5400.00	3800.00	289.60
T_{DNA} [s]	10.00	9.98	14.54
D_{inj} [cm]	2.00	1.47	1.52

5. Conclusions

Improvements of gene electrotranfer protocol are becoming of paramount importance to translate this treatment into human patients. When DNA plasmid vector is injected into tissues, its expression is limited, due to the presence of ECM and cell membrane barriers. The use of hyaluronidase, which allows a partial digestion of the ECM, and EP - a physical methodology favoring cell membrane permeabilization - represents a valid platform for DNA delivery expression. In this study, a mathematical model simulating the core part of the delivery protocol has been applied in order to enhance the DNA expression, identifying the best

injection and waiting time for the DNA administration. Once numerically compared with the standard operative protocol, the optimal parameters obtained by our algorithms consist of an injection localisation about 1–2 cm deep, an injection time for both hyaluronidase and DNA of about 10s and a waiting time between the two injections below 300 s. According to our simulations improvement of about 30% of the effective area of DNA is achievable, which could lead to a much better gene expression than in the standard protocol. Ideally the electroporation should be performed less than 1 min after the end of the DNA injection.

These numerical results will be confirmed (or not) by forthcoming dedicated experiments *in vivo* to compare the standard protocol proposed in Chiarella and Signori (2014) with our optimized protocols. This would also be a decisive aid in the transfer of this medical approach from bench to clinical applications.

The application of this optimization procedure can take also into account the peculiarities of the different patients, through the specific mechanical and morphological characteristics of the tissues (personalized medicine).

The reduced diffusion of plasmid DNA into the tissue has been also evidenced by this study: a possible solution to this problem could be the adoption of multiple-site injections. This strategy, possibly in combination with a CNC syringe for the exact actuation of the protocol, could allow the plasmid DNA to reach areas of the tissue where the hyaluronidase has produced its effects.

6. Acknowledgements

M.D. has been partly granted by Université Franco-Italienne, Project VINCI C2-25. M.D. and C.P. are partly granted by the Plan Cancer projects DYNAMO (Inserm 9749) and NUMEP (Inserm 11099). This study has been carried out within the scope of the Inria Associate Team Num4SEP.

References

Aihara, H. and Miyazaki, J.-I. (1998). Gene transfer into muscle by electroporation in vivo. *Nature Biotechnology*, 16:867–870.

Akerstrom, T., Vedel, K., Needham, J., and Hojman, P. (2015). Optimizing hyaluronidase dose and plasmid DNA delivery greatly improves gene electrotransfer efficiency in rat skeletal muscle. *Biochemistry and Biophysics Reports*.

Al-Dosari, M. S. and Gao, X. (2009). Nonviral gene delivery: Principle, limitations, and recent progress. *The AAPS Journal*, 11:671–681.

Ambrosi, D., Lancellotta, R., and Preziosi, L. (2002). Mathematical models for soil consolidation problems : a state of the art report. *Chapter 6 of Modeling and Mechanics of Granular and Porous Materials*, pages 159–180.

André, F. M., Cournil-Henrionnet, C., Vernerey, D., Opolon, P., and Mir, L. M. (2006). Variability of naked dna expression after direct local injection: the influence of the injection speed. *Gene Therapy*, 13(23):1619–1627.

André, F. M. and Mir, L. M. (2004). Dna electrotransfer: its principles and an updated review of its therapeutic applications. *Gene therapy*, 11 Suppl 1:S33–42.

Barthelemy, J. F. M. and Haftka, R. T. (1993). Approximation concepts for optimum structural design - a review. *Structural optimization*, 5(3):129–144.

Barton, R. R. and Meckesheimer, M. (2006). Chapter 18 metamodel-based simulation optimization. In Henderson, S. G. and Nelson, B. L., editors, *Simulation*, volume 13 of *Handbooks in Operations Research and Management Science*, pages 535 – 574. Elsevier.

Baxter, L. T. and Jain, R. K. (1989). Transport of fluid and macromolecules in tumors. i. role of interstitial pressure and convection. *Microvascular research*.

Buhren, B. A., Schrumpf, H., Hoff, N.-P., Bölke, E., Hilton, S., and Gerber, P. A. (2016). Hyaluronidase: from clinical applications to molecular and cellular mechanisms. *European journal of medical research*, 21(1):5.

Bureau, M. F., Naimi, S., Ibad, T. R., and Seguin, J. (2004). Intramuscular plasmid DNA electrotransfer: biodistribution and degradation. *Biochimica et Biophysica Acta (BBA)*.

Chapelle, D. and Moireau, P. (2014). General coupling of porous flows and hyperelastic formulations. from thermodynamics principles to energy balance and compatible time schemes. *European Journal of Mechanics - B/Fluids*, 46(Supplement C):82 – 96.

Chiarella, P., De Santis, S., Fazio, V. M., and Signori, E. (2013a). Hyaluronidase contributes to early inflammatory events induced by electrotransfer in mouse skeletal muscle. *Human Gene Therapy*, 24(4):406–416.

Chiarella, P., Fazio, V. M., and Signori, E. (2013b). Electroporation in dna vaccination protocols against cancer. *Current Drug Metabolism*, 14(3):291–299.

Chiarella, P. and Signori, E. (2014). Intramuscular DNA vaccination protocols mediated by electric fields. In Shulin, L., Jeffry, C., Richard, H., and Justin, T., editors, *Electroporation Protocols*, volume 1121 of *Methods in Molecular Biology*, pages 315 – 324. Humana Press.

De Robertis, M., Pasquet, L., Loiacono, L., Bellard, E., Messina, L., Vaccaro, S., Di Pasquale, R., Fazio, V. M., Rols, M.-P., Teissi'e, J., Golzio, M., and Signori, E. (2018). In vivo evaluation of a new recombinant hyaluronidase to improve gene electro-transfer protocols for dna-based drug delivery against cancer. *Cancers*, 10(11):1–20.

Deville, M. (2017). *Mathematical model of enhanced drug delivery by mean of electroporation or enzymatic treatment*. PhD thesis, Université de Bordeaux & Università di Roma Tor Vergata.

Deville, M., Natalini, R., and Poignard, C. (2018). A continuum mechanics model of enzyme-based tissue degradation in cancer therapies. *Bulletin of Mathematical Biology*, 80(12):3184–3226.

Fusi, L., Farina, A., and Ambrosi, D. (2006). Mathematical Modeling of a Solid–Liquid Mixture with Mass Exchange Between Constituents. *Mathematics and Mechanics of Solids*, 11(6):575–595.

Geuzaine, C. and Remacle, J.-F. (2009). Gmsh: A 3-d finite element mesh generator with built-in pre- and post-processing facilities. *International Journal for Numerical Methods in Engineering*, 79(11):1309–1331.

Girish, K. S. and Kemparaju, K. (2007). The magic glue hyaluronan and its eraser hyaluronidase: a biological overview. *Life sciences*, 80(21):1921–1943.

Hardee, C. L., Arévalo-Soliz, L. M., Hornstein, B. D., and Zechiedrich, L. (2017). Advances in non-viral dna vectors for gene therapy. *Genes*, 8(2).

Hecht, F. (2012). New development in FreeFem++. *Journal of Numerical Mathematics*, 20(3-4):251–265.

Hedayat, A. S., Sloane, N. J. A., and Stufken, J. (1999). *Orthogonal Arrays: Theory and Applications*. Springer-Verlag, New York.

Lang, G. E., Vella, D., Waters, S. L., and Goriely, A. (2016). Mathematical modelling of blood-brain barrier failure and oedema. *Mathematical medicine and biology : a journal of the IMA*.

Leguèbe, M., Notarangelo, M. G., Twarogowska, M., Natalini, R., and Poignard, C. (2017). Mathematical model for transport of dna plasmids from the external medium up to the nucleus by electroporation. *Mathematical Biosciences*, 285(Supplement C):1 – 13.

McMahon, J. M., Signori, E., Wells, K. E., Fazio, V. M., and Wells, D. J. (2001). Optimisation of electrotransfer of plasmid into skeletal muscle by pretreatment with hyaluronidase - increased expression with reduced muscle damage. *Gene Therapy*, 8:1264–1270.

Notarangelo, M. G., Natalini, R., and Signori, E. (2014). Gene therapy: the role of cytoskeleton in gene transfer studies based on biology and mathematics. *Current Gene Therapy*, 14(2):121–127.

Peri, D. (2009). Self-learning metamodels for optimization. *Ship Technology Research*, 56(3):95–109.

Peri, D. (2018). Easy-to-implement multidimensional spline interpolation with application to ship design optimisation. *Ship Technology Research*, 65(1):32–46.

Pucihar, G., Krmelj, J., Reber**v**sek, M., Napotnik, T. B., and Miklav**v**ci**v**c, D. (2011). Equivalent pulse parameters for electroporation. *IEEE Transactions on Biomedical Engineering*, 58(11):3279–3288.

Rols, M., Delteil, C., Golzio, M., Dumond, P., Cros, S., and J, T. (1998). In vivo electrically mediated protein and gene transfer in murine melanoma. *Nature Biotechnology*, 16(2):168–171.

Schertzer, J. D., Plant, D. R., and Lynch, G. S. (2006). Optimizing plasmid-based gene transfer for investigating skeletal muscle structure and function. *Molecular Therapy*, 13(4).

Shu, L., Jiang, P., Wan, L., Zhou, Q., Shao, X., and Zhang, Y. (2017). Metamodel-based design optimization employing a novel sequential sampling strategy. *Engineering Computations*, 34(8):2547–2564.

Soltani, M. and Chen, P. (2012). Effect of tumor shape and size on drug delivery to solid tumors. *Journal of biological engineering*.

Swartz, M. A. and Fleury, M. E. (2007). Interstitial flow and its effects in soft tissues. *Annual review of biomedical engineering*, 9:229–256.

Toropov, V. V. (1995). *Multipoint Approximation Method for Structural Optimization Problems with Noisy Function Values*, pages 109–122. Springer Berlin Heidelberg, Berlin, Heidelberg.

Ward, S. R. and Lieber, R. L. (2005). Density and hydration of fresh and fixed human skeletal muscle. *Journal of biomechanics*, 38(11):2317–2320.

Wolff, J. A., Malone, R. W., Williams, P., Chong, W., Acsadi, G., Jani, A., and Felgner, P. L. (1990). Direct gene transfer into mouse muscle in vivo. *Science (New York, N.Y.)*, 247(4949 Pt 1):1465–1468.

Yao, W., Li, Y., and Ding, G. (2012). Interstitial fluid flow: the mechanical environment of cells and foundation of meridians. *Evidence-based complementary and alternative medicine : eCAM*, 2012:853516.

Zöllner, A. M., Abilez, O. J., Böl, M., and Kuhl, E. (2012). Stretching skeletal muscle: chronic muscle lengthening through sarcomerogenesis. *PloS one*, 7(10):e45661.